Inorganic Chemistry

Article

pubs.acs.org/IC

Dicopper Double-Strand Helicates Held Together by Additional $\pi-\pi$ Interactions

Massimo Boiocchi,[‡] Valentina Brega,[†] Carlo Ciarrocchi,[†] Luigi Fabbrizzi,*[,†] and Piersandro Pallavicini[†]

[†]Dipartimento di Chimica and [‡]Centro Grandi Strumenti, Università di Pavia, 27100 Pavia, Italy

Supporting Information

ABSTRACT: The bis-bidentate ligand, obtained from Schiff base condensation of *RR*-1,2-cyclohexanediamine and 8-naphthylmethoxyquinoline-2-carbaldehyde (**L−L**), forms with $[Cu^{I}(MeCN)_4]ClO_4$ a double strand helicate complex, made especially stable by the presence of four definite interstrand $\pi-\pi$ interactions involving a quinoline subunit and a naphthylmethoxy substituent of the two strands. The $[Cu^{I}_2(\mathbf{L-L})_2]^{2+}$ complex, which does not decompose even on excess addition of either **L−L** or Cu^{I}, undergoes a two electron oxidation in MeCN, through two one-electron fully reversible steps, separated by 260 mV, as shown by cyclic voltammetry (CV) studies. The high stability of the mixed valence complex $[Cu^{I}Cu^{II}(\mathbf{L-L})_2]^{3+}$ with respect to disproportionation to $[Cu^{I}_2(\mathbf{L-L})_2]^{2+}$ and $[Cu^{II}_2(\mathbf{L-L})_2]^{4+}$ is essentially due to a favorable electrostatic term. Cu^{II} forms with **L−L** a stable species, with a 1:1 stoichiometric ratio, but, in the absence of crystallographic data, it was impossible to assess whether it is of mono- or dinuclear nature. However, CV studies on an MeCN solution containing equimolar amounts of Cu^{II} and **L−L** showed the presence in the reduction scan of two fully reversible waves, separated by about 250 mV, which indicated the presence in solution of a dicopper(II) double strand helicate complex, $[Cu^{II}_2(\mathbf{L-L})_2]^{4+}$. This work demonstrates that additional interstrand $\pi-\pi$ interactions can favor the formation of unusually stable dicopper(I) and dicopper(II) helicate complexes.

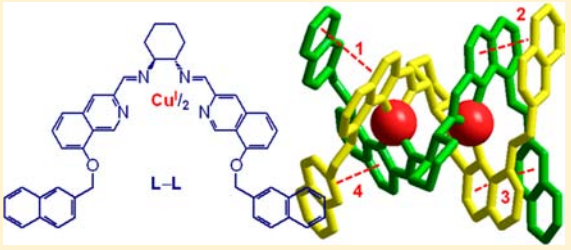

INTRODUCTION

Pairs of molecular strands often arrange themselves according to a double-helical pattern. Such a process is driven by the willingness of the two molecules to establish as many intermolecular bonding interactions as possible, under a regime of minimized steric repulsions. The formation of the intricate double helical structure is achieved through a repetitive trial-and-error mechanism, and is associated with the establishment of fast and reversible noncovalent interactions and, above all, hydrogen bonding. In fact, the most known and elaborate example of an H-bond controlled double-helical arrangement is that of DNA.[1] Also metal−ligand interactions may possess convenient features of fast reversibility, suitable for the formation of double helices.[2] As an example, two linear multidentate ligands, under the appropriate conditions, can wrap around two or more metal centers to give polynuclear double-strand helicate complexes. Each metal ion acts as a template and represents an integral part of the double helix, which disassembles on metal removal. Metal ions with a d^{10} electronic configuration (e.g., Cu^{I}, Ag^{I}) have a strong preference for a tetrahedral coordination, a geometrical arrangement which possesses a helical twist,[3] and tend to form double strand helicate complexes. In particular, *n* d^{10} metal ions M^{+} will favor the assembling of two linear molecules **X** containing *n* bidentate subunits, to give an $[M_n^{I}(\mathbf{X})_2]^{n+}$ helicate.[4] Moreover, d^{10} metal ions form stable complexes with π-acceptor ligands, which explains why most of the reported helicates (including the very first examples) involved multidentate ligands containing the 2,2′-bipyridine subunit, and, less frequently, other unsaturated nitrogen heterocycles.

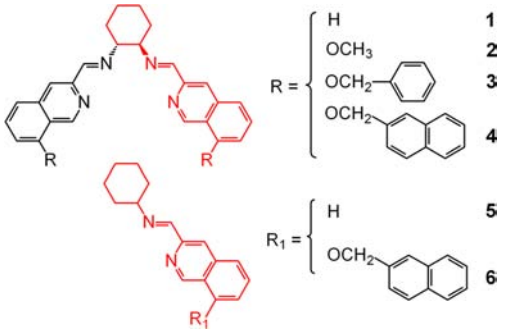

Among systems not based on polypyridines, a particular case is represented by the bis-bidentate ligands obtained from the Schiff base condensation of 1,2-diamino-cyclohexane with 2 equiv of 2-pyridine carbaldehyde.[5] In our laboratory, we first considered the reaction of 1,2-diamino cyclohexane with 2-quinoline-carbaldehyde, to give **1**.[6] The Schiff base obtained from *trans*-1,2-diaminocyclohexane, in its racemic form (^{rac}L∩L), on reacting with Cu^{I}, can give rise (i) to the double helix dinuclear complex, and (ii) to a nonhelical (side-by-side) dinuclear complex. In particular, the double-helical complex exists as a racemic mixture of homochiral complexes *M,M*-

Received: July 1, 2013
Published: September 4, 2013

$[Cu_2^I(^{RR}L\cap L)_2]^{2+}$ (i.e., a double helix with *M* handedness) and *P,P*-$[Cu_2^I(^{SS}L\cap L)_2]^{2+}$ (i.e., a double helix with *P* handedness), which establishes the general principle of homochiral recognition. On the other hand, the side-by-side form contains two ligands L∩L of inverted chirality: $[Cu_2^I(^{RR}L\cap L)(^{SS}L\cap L)]^{2+}$. The two arrangements, whether helical or side-by-side, have a comparable stability, and can be isolated as solids in one form or in the other, depending upon the counteranion used or crystallization conditions. In contrast, when starting from the *cis* form of 1,2-diaminocyclohexane, whether *R,R* or *S,S*, only the corresponding homochiral helicate complexes are obtained, as demonstrated in a number of studies on copper(I) complexes with bis-bidentate ligands of the same class.[7]

In addition to metal−ligand interactions, other interactions can contribute to the stability of the $[Cu_2^I(L\cap L)_2]^{2+}$ helicate. This was the case of the dinuclear complex of the Schiff base ^{RR}**3**, whose crystal structure showed the existence of two well-defined interstrand $\pi-\pi$ interactions, each involving one pyridine ring of one strand and a benzyloxy ring of the other (see Figure 1).[8]

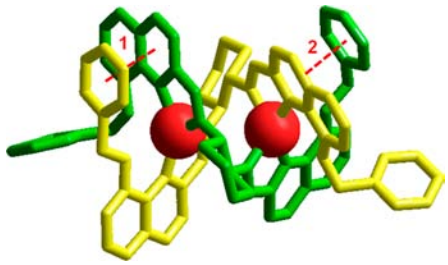

Figure 1. Crystal structure of the $[Cu_2^I(^{RR}\mathbf{3})_2]^{2+}$ complex.[8] A given color (whether green or yellow) has been assigned to each strand. Red dashed lines indicate the two interstrand $\pi-\pi$ interactions between a pyridine ring of one strand and a benzyloxy subunit of the other.

We report here a study on the dicopper(I) complex of the Schiff base bis-bidentate ligand ^{RR}**4**, containing a 2-naphtyloxy substituent, potentially capable of establishing more extended $\pi-\pi$ interactions. The presence of such interactions has been demonstrated by the crystal structure of $[Cu_2^I(^{RR}\mathbf{4})_2](ClO_4)_2$. The stability of the $[Cu_2^I(^{RR}\mathbf{4})_2]^{2+}$ complex in solution has been investigated through UV−vis titration experiments and compared to that of the mononuclear copper(I) with the bidentate ligand **6**, to be considered as one-half of helicand **4**, which allowed us to verify the existence of a thermodynamic helicate effect. Moreover, the Cu^I/Cu^{II} redox change in MeCN has been investigated through voltammetry studies at the platinum electrode. Also in this case, $\pi-\pi$ interactions seem to play a significant role, stabilizing the double helix arrangement for the Cu^{II} oxidation state in solution.

EXPERIMENTAL SECTION

General Procedures and Materials. All reagents for syntheses were purchased form Aldrich/Fluka and used without further purification. $[Cu^I(CH_3CN)_4]ClO_4$ was prepared by literature method,[9] and recrystallized from MeCN prior to use. All reactions were performed under N_2.

UV/vis spectra were recorded on a Varian CARY 100 spectrophotometer with quartz cuvettes of the appropriate path length (0.1 or 1 cm). In any case, the concentration of the chromophore and the optical path were adjusted to obtain spectra with AU ≤ 1.

^{1}H NMR were obtained, at 298 K, on a Bruker Avance 400 spectrometer (400 MHz) operating at 9.37 T. Mass spectra were acquired on a Thermo-Finnigan ion trap LCQ Advantage Max instrument, equipped with an ESI source.

Electrochemical Measurements. Electrochemical measurements were performed on a BAS 100B/W instrument. MeCN was freshly distilled from CaH_2 under a N_2 atmosphere and made 0.1 M in $[Bu_4N]ClO_4$. In the voltammetry experiments, a three-electrode cell was used with a platinum electrode as the working electrode, silver/silver ion as a reference (clean silver wire into an electrode filling solution of MeCN, made 1×10^{-2} M in $AgNO_3$ and 0.1 M in $[Bu_4N]ClO_4$) and a platinum coil as the auxiliary electrode. The reference electrode was calibrated toward the ferrocenium/ferrocene couple (Fc^+/Fc).

X-ray Crystallographic Studies. The $[Cu_2^I(^{RR}\mathbf{4})_2](ClO_4)_2\cdot 4CH_3CN\cdot 2H_2O$ complex salt formed as dark-blue platy crystals of poor X-ray diffraction quality, also for the decay occurring during the data collection at ambient condition. To prevent crystal decay, the selected single crystal was placed in a closed glass capillary with a small amount of mother liquor. Diffraction data were collected by means of a Bruker-AXS CCD-based diffractometer, working at ambient condition with graphite-monochromatized $Mo_{K\alpha}$ X-radiation (γ = 0.71073 Å). However, diffraction data having θ angle greater than 21° remained unobservable. Crystal data for the $[Cu_2^I(^{RR}\mathbf{4})_2](ClO_4)_2\cdot 4CH_3CN\cdot 2H_2O$ crystal are $C_{104}H_{94}Cl_2Cu_2N_{12}O_{13}$; *M* 1917.90; dimension 0.48 × 0.32 × 0.08 mm; hexagonal, $P6_4$ (no. 172); *a* 14.007(4), *c* 40.837(12) Å; *V* 6939(5) Å^3; *Z* = 3; ρ_{calcd} 1.377 g cm^{-3}; μ $Mo_{K\alpha}$ 0.589 mm^{-1}; θ range 2−20.8°; 28548 measured reflections; 4784 unique reflections (R_{int} 0.052); 4034 strong data [$I_o > 2\sigma(I_o)$]; 602 refined parameters; 0.0603 and 0.1519 *R*1 and *wR*2 for strong data; 0.0735 and 0.1623 *R*1 and *wR*2 for all data; GOF = 1.134; 0.51 and −0.31 eÅ^{-3} max and min residuals.

Data reductions (including intensity integration, background, Lorentz and polarization corrections) were performed with the SAINT software;[10] absorption effects were empirically evaluated by the SADABS software,[11] and absorption correction was applied to the data (min./max. transmission factors were 0.54/0.98). Crystal structure was solved by direct methods (SIR 97)[12] and refined by full-matrix least-squares procedures on F^2 using all reflections (SHELXL 97).[13] Anisotropic displacement parameters were refined for all non-hydrogen atoms. All hydrogens were placed at calculated positions with the appropriate AFIX instructions and refined using a riding model; positions for hydrogens belonging to water molecules remained undetermined.

The poor X-ray diffraction quality of the single crystal imposed the use of soft restraint during the terminal least-squares cycles of refinement, to prevent the convergence of the crystallographic parameters toward a final model showing chemically inappropriate features. In particular, the C−C distances for atoms forming the terminal naphthalene double rings were restrained to be 1.39 ± 0.01 Å (with DFIX instructions) and the two independent naphthalene groups of the asymmetric unit were restrained to show the same geometries using the SAME instruction. Further restrains on the U_{ij} parameters (DELU and ISOR instructions) were used for several atoms of the two independent naphthalene groups.

Syntheses: 2-Methyl-8-(naphthalen-2-ylmethoxy)quinoline (7). A 2.2 g portion of freshly cut sodium (0.096 mol) were dissolved in 100 mL of stirred isopropanol. The solution was heated to reflux to complete dissolution of the metal. Ten grams of powdered 2-methyl-8-hydroxyquinoline (0.063 mol) were added, to give a bright yellow precipitate. A 14.4 g portion of 2-bromomethylnaphthalene (0.065 mol) was then added over a period of 1 h.

The reaction mixture was heated to reflux for 16 h. The white NaBr precipitate was filtered off and washed with isopropanol. The greenish alcoholic solution was then rotovaporated to give a green oil, which solidified upon cooling. The solid was triturated in 500 mL of water three times, and the powdered green solid was desiccated in a vacuum oven at 50 °C overnight. (16.9 g, 0.056 mol, 90%). $C_{21}H_{17}NO$ MW = 299.13; ESI-MS: positive ions, *m/z* = 300.2 $[M+H]^+$ (100%), 599.9

dx.doi.org/10.1021/ic401684u | Inorg. Chem. 2013, 52, 10643−10652

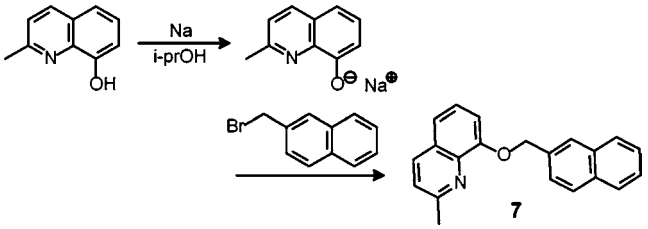

$[2M+H]^+$ (70%). Elemental analysis. Calc. For $C_{21}H_{17}NO$: C, 84.25; H, 5.62; N, 4.68. Found: C, 84.10; H, 5.70; N, 4.62%.

8-/Naphthalen-2-ylmethoxy)quinoline-2-carbaldehyde (8). A solution of **7** (10 g, 0.033 mol) in 35 mL of 1,4-dioxane was added dropwise to a vigorously stirred suspension of SeO_2 (5 g, 0.045 mol) in 25 mL of 1,4-dioxane, which was kept at 60 °C. Stirring and heating were maintained for 4 h. After cooling, the brick red solution was filtered to eliminate the black powder of selenium and rotovapored to dryness. The red solid residue was extracted with 3 × 150 mL portions of hot cyclohexane, from which 5.7 g of **8** crystallized on cooling (yield: 55.4%).

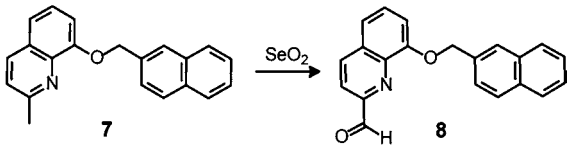

$C_{21}H_{15}NO_2$ MW = 313.11: ESI-MS: positive ions, m/z = 346.3 $[M+H+CH_3OH]^+$ (100%), 368.2 $[M+CH_3OH+Na]$ (25%), 690.9 $[2M+2CH_3OH]^+$ (90%), 713.0 $[2M+2CH_3OH+Na]^+$ (80%). Elemental analysis. Calc. For $C_{21}H_{17}NO$: C, 80.49; H, 4.82; N, 4.47. Found: C, 80.39; H, 4.88; N, 4.41%.

Schiff Base ^{RR}4. To a solution of **8** (1 g, 0.00319 mol) in 75 mL of MeOH, 0.182 g (0.00159 mol) of 1*R*,2*R*-cyclohexanediamine were

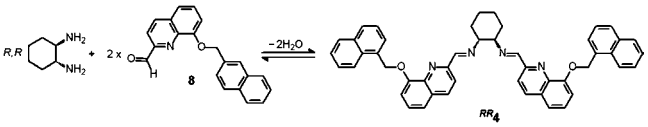

added in small portions under stirring. Stirring at room temperature was maintained for 24 h. On rotovaporation, a brown solid residue was obtained, which was dissolved in $CHCl_3$. On MeCN addition, a pale brown microcrystalline solid formed, which was separated by filtration and dried over P_4O_{10} (0.4 g, 0.57 mmol; yield: 35.7%). $C_{48}H_{40}N_4O_2$ MW = 704.32. ESI-MS: positive ions: m/z = 705.3 $[M+H]^+$ (100%), 1409.9 $[2M+H]^+$ (20%).

^{1}H NMR (in CD_3CN): δ = 1.24−1.37 ppm (m, 4H); 1.54−1.66 ppm (m, 4H); 3.61−3.70 ppm (m, 2H); 5.43 ppm (s, 4H); 7.21 ppm (d, 2H); 7.36−7.47 ppm (m, 4H); 7.49−7.55 ppm (m, 4H); 7.61 ppm (d, 2H), 7.86−8.12 ppm (m, 12H), 8.42 ppm (s, 2H). Elemental analysis. Calc. For $C_{48}H_{40}N_4O_2$: C, 81.79; H, 5.72; N, 7.95. Found: C, 81.72; H, 5.78; N, 7.91%.

Crystals of the $[[Cu_2^I(^{RR}4)_2](ClO_4)_2{\cdot}4CH_3CN{\cdot}2H_2O$ complex salt, of dark blue color, were obtained through slow evaporation (at 4 °C) of an MeCN solution containing equimolar amounts of ^{RR}**4** and $[Cu^I(CH_3CN)_4]ClO_4$. In the electrochemical studies, MeCN solutions of the Cu^I and Cu^{II} complexes were prepared by mixing equimolar amounts of ^{RR}**4** and of the pertinent copper salt, $[Cu^I(CH_3CN)_4]ClO_4$ and $Cu^{II}(CF_3SO_3))_2$, at the 10^{-3} M scale, which, because of the high solution stability, ensured the quantitative formation of the corresponding complexes (vide infra).

RESULTS AND DISCUSSION

1. Crystal and Molecular Structure of the $[Cu_2^I(^{RR}4)_2]^{2+}$ Helicate Complex. The crystal of the hydrate $[Cu_2^I(^{RR}4)_2]^-(ClO_4)_2$ salt contains additional acetonitrile solvent molecules, and it shows the symmetry of the chiral enantiomorphic $P6_4$ space group. The final Flack's parameter of 0.09(3) confirms that the crystal contains only the enantiomer of ligand **4** in the *R*,*R* form, two of which originate a double helix kept together by two chelate Cu^I ions. The homochiral double-helix shows *M* handedness, while a plot showing thermal ellipsoids and a tube representation of the *M*,*M*-$[Cu_2^I(^{RR}4)_2]^{2+}$ molecular cation are reported in Figure 2.

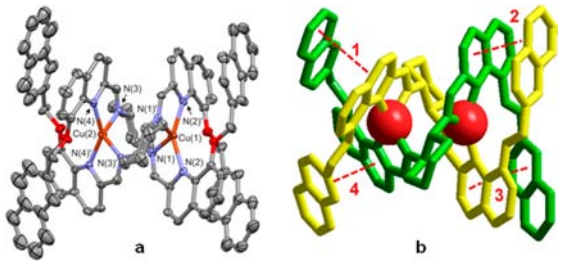

Figure 2. (a) Plot showing thermal ellipsoids of the *M*,*M*-$[Cu_2^I(^{RR}4)_2]^{2+}$ helicate cationic complex (ellipsoids are drawn at the 20% probability level, atom name are reported only for the metal centers and for the bonded N atoms, symmetry code: (′) = −*x*, 1−*y*, *z*). (b) A tube representation of the *M*,*M*-$[Cu_2^I(^{RR}4)_2]^{2+}$ helicate complex is drawn with different colors for the two symmetrically equivalent strands; the homochiral double helix shows *M* handedness and extensive interstrand $\pi-\pi$ interactions (dashed lines).

The asymmetric unit of the helicate complex is made by only one complete ^{RR}**4** strand and by the couple of metal centers. The two symmetrically equivalent strands are related by a 2-fold rotation axis passing through the two metal centers, and each Cu^I center is tetrahedrally coordinated by four N atoms belonging to the imine and quinoline groups. Selected Cu−N bond distances and angles are reported in Table 1. The Cu−N(imine) and Cu−N(quinoline) distances are very similar, and the values for Cu(1) center are only a bit long, being the mean Cu−N distance of 2.04(1) and 2.01(1) Å for Cu(1) and Cu(2) centers, respectively. Similar distances occur for the helicate complex $[Cu_2^I(^{RR}3)_2]^{2+}$, in which the four Cu−N distances are in the range 2.02(1)−2.08(1) Å. However, the tetrahedral Cu^I coordination for the $[Cu_2^I(^{RR}4)_2]^{2+}$ molecular cation is a bit more distorted than in the $[Cu_2^I(^{RR}3)_2]^{2+}$ one, as evidenced by the dihedral angle θ between the planes containing the five-membered chelate rings Cu−N−C−C−N. The angles θ in the $[Cu_2^I(^{RR}4)_2]^{2+}$ molecular cation are 70.8(2) and 72.6(2)° for Cu(1) and Cu(2), respectively, whereas it is 76.9(1)° for the couple of symmetrically equivalent metal centers in the $[Cu_2^I(^{RR}3)_2]^{2+}$ molecular cation (θ is 0° or 180° for a square planar coordination geometry; 90° for tetrahedral coordination geometry).

The naphthylmethoxy groups are excluded by any coordinative interactions with the Cu^I centers, the four proper O atoms being placed at 2.91(1) Å (twice) from the Cu(1) center and at 2.84(1) Å (twice) from the Cu(2) center. Similar Cu−O distances have been observed in the $[Cu_2^I(^{RR}3)_2]^{2+}$ helicate molecular cation,[8] in which the Cu−O distances fall in the range 2.79(1)−2.89(1) Å. However, in the two helicate complexes the couples of Cu^I metal centers are separated by slightly different distances, the Cu−Cu distance being 3.84(1) in $[Cu_2^I(^{RR}4)_2]^{2+}$ and 3.89(1) Å in $[Cu_2^I(^{RR}3)_2]^{2+}$ (see discussion below).

Actually, the $[Cu_2^I(^{RR}3)_2]^{2+}$ helicate molecular cation exhibits C_2 symmetry,[8] and only two phenyl rings are face-to-face stacked with respect to two adjacent quinoline moieties, thus originating *two* interstrand $\pi-\pi$ interactions (see Figure 1). On

dx.doi.org/10.1021/ic401684u | Inorg. Chem. 2013, 52, 10643−10652

Table 1. Selected Bond Distances (Å) and Angles (deg) around the Two Cu^I Centers in $[Cu_2^I(^{RR}4)_2]^{2+}$ Molecular Cation[a]

Cu(1)–N(1)	2.038(7)	Cu(2)–N(3)	2.011(6)
Cu(1)–N(2)	2.040(7)	Cu(2)–N(4)	2.009(7)
N(1)–Cu(1)–N(2)	82.4(3)	N(3)–Cu(2)–N(4)	83.6(3)
N(1)–Cu(1)–N(1)′	124.2(4)	N(3)–Cu(2)–N(3)′	123.0(4)
N(1)–Cu(1)–N(2)′	113.4(3)	N(3)–Cu(2)–N(4)′	113.6(3)
N(2)–Cu(1)–N(2)′	147.0(4)	N(4)–Cu(2)–N(4)′	144.6(4)

[a]Symmetry code: (′) = −x, 1−y, z.

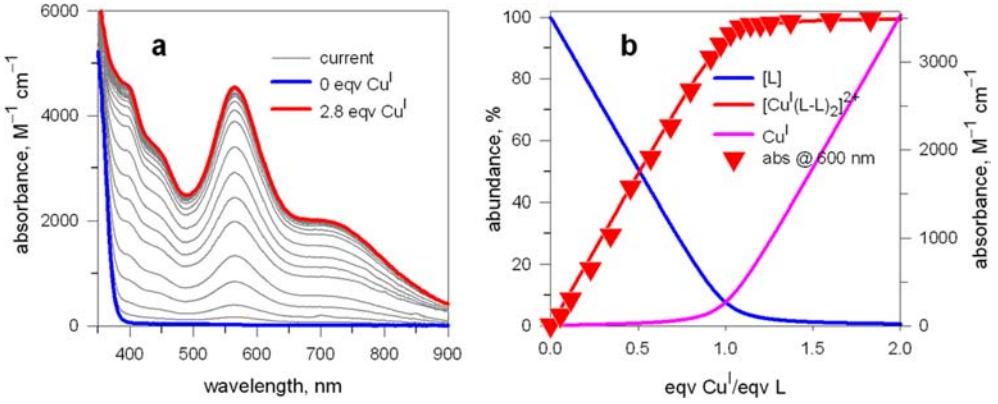

Figure 3. (a) Absorption spectra taken over the course of the titration of an MeCN solution 9.99×10^{-5} M of $^{RR}4$ with a standard solution 1.03×10^{-2} M in $[Cu^I(MeCN)_4]ClO_4$; (b) lines: concentration profiles (% with respect to L∩L = $^{RR}4$) of the species at the equilibrium; symbols: molar absorbance at 600 nm.

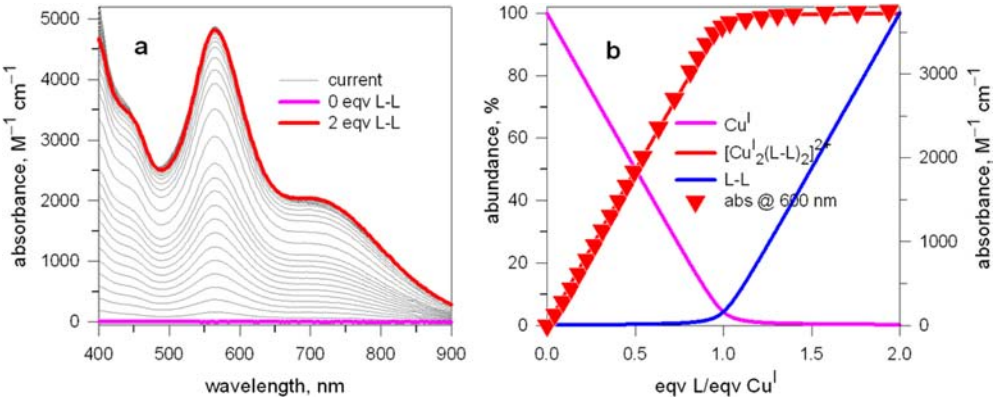

Figure 4. (a) Absorption spectra taken over the course of the titration of an MeCN solution 1.04×10^{-4} M of $[Cu^I(MeCN)_4]ClO_4$ with a standard solution 1.03×10^{-2} M in $^{RR}4$ (= L∩L); (b) lines: concentration profiles (% with respect to Cu^I) of the species at the equilibrium; symbols: molar absorbance at 600 nm.

the contrary, the $[Cu_2^I(^{RR}4)_2]^{2+}$ helicate molecular cation exhibits D_2 symmetry, and all the four naphthalene rings are face-to-face stacked with respect to the four adjacent quinoline moieties, thus originating *four* interstrand $\pi-\pi$ interactions (see Figure 2). The dihedral angles between the naphthalene and quinoline best planes, the centroid-centroid distances and the closest C···C contacts characterizing the four face-to-face $\pi-\pi$ stacking interactions are 2.5(3)°, 3.51(2) Å, and 3.38(2) Å, respectively, for the first kind of $\pi-\pi$ interaction occurring twice, and are 5.0(5)°, 3.57(2) Å, and 3.37(2) Å for the second kind of $\pi-\pi$ interaction occurring twice. Notice that the corresponding values for the two equivalent $\pi-\pi$ interactions between phenyl ring and quinoline group in the $[Cu_2^I(^{RR}3)_2]^{2+}$ helicate complex are 3.7(2)°, 4.06(1) Å, and 3.43(1) Å. As expected, the 2-naphtylmethoxy substituent favors the formation of extensive interstrand $\pi-\pi$ interactions.

2. Solution Stability of the $[Cu_2^I(^{RR}4)_2]^{2+}$ Helicate Complex. The formation of the double strand helicate complex $[Cu_2^I(^{RR}4)_2]^{2+}$ in solution was investigated by carrying out UV–vis titration experiments in MeCN. In particular, a solution 9.99×10^{-5} M in $^{RR}4$ was titrated with a standard solution of $[Cu^I(MeCN)_4]ClO_4$ in MeCN. The family of spectra obtained over the course of the titration is shown in Figure 3a.

On Cu^I addition, two intense bands developed at 565 and 715 nm, which originate from metal-to-ligand charge-transfer (MLCT) transitions typically observed for Cu^I in a four-coordinating imine-pyridine donor set. These bands reached saturation for a $Cu^I/^{RR}4$ molar ratio of 1. Best fitting of spectrophotometric titration data over the 400–900 nm wavelength interval, using a nonlinear least-squares procedure,[14] was obtained by assuming the occurrence of the equilibrium (L∩L = $^{RR}4$)

dx.doi.org/10.1021/ic401684u | Inorg. Chem. 2013, 52, 10643–10652

Table 2. log *K* Values for Equilibria in MeCN, at 25°C, Involving Cu^I and Helicands ^{RR}2, ^{RR}3, and ^{RR}4 (L∩L) and Cu^I and the Bidentate Ligands 5 and 6 (L)

	equilibrium	$^{RR}2^a$	$^{RR}3^b$	$^{RR}4^c$	5^c	6^c
log K_{21}	$Cu^I + 2L∩L \leftrightarrows [Cu^I(L∩L)_2]^+$	11.0	10.1			
log K_{22}	$2Cu^I + 2L∩L \leftrightarrows [Cu^I_2(L∩L)_2]^{2+}$	17.4	16.0	16.1(1)^d		
log K'_{11}	$Cu^I + L \leftrightarrows [Cu^IL]^+$				5.1(1)^d	4.8(1)^d
log K'_{21}	$[Cu^IL]^+ + L \leftrightarrows [Cu^IL_2]^+$				5.0(1)^d	4.8(2)^d

[a]Ref 7f. [b]Ref 8. [c]This work; in parentheses the uncertainty on the last figure. [d]Average value from L∩L + Cu^I titration and from Cu^I + L∩L titration. [d]Average value from L + Cu^I titration and from Cu^I + L titration.

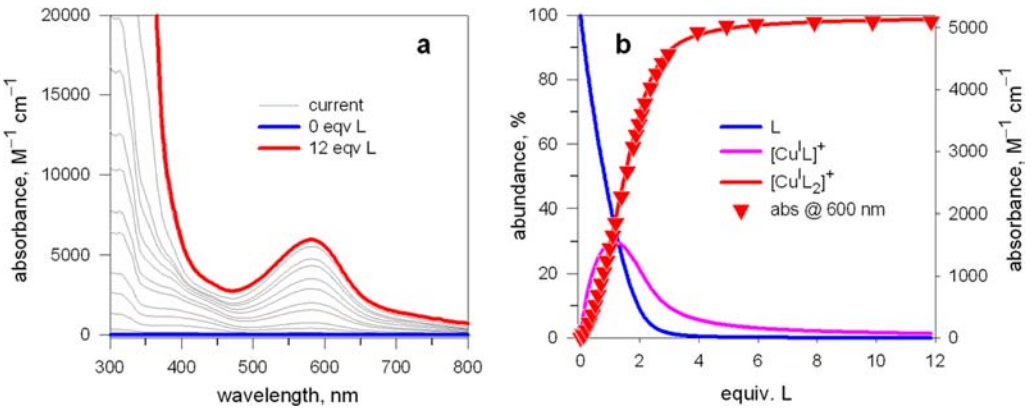

Figure 5. (a) Absorption spectra taken over the course of the titration of an MeCN solution 1.006×10^{-4} M of $[Cu^I(MeCN)_4]ClO_4$ with a standard solution 1.014×10^{-2} M in **6** (= L); (b) lines: concentration profiles (% with respect to Cu^I) of the species at the equilibrium; symbols: molar absorbance at 600 nm.

$$2Cu^+ + 2L ∩ L \leftrightarrows [Cu^I_2(L ∩ L)_2]^{2+} \quad (1)$$

to which corresponds a log K_{22} = 16.12 ± 0.03. Any attempt to introduce further equilibria, for instance of type (2)

$$Cu^+ + 2L ∩ L \leftrightarrows [Cu^I(L ∩ L)_2]^+ \quad (2)$$

was rejected by the least-squares minimization program. Figure 2b shows the concentration profiles of the species present at the equilibrium over the course of the titration: L∩L, $[Cu^I_2(L∩L)_2]^{2+}$ and Cu^I. On first addition of $[Cu^I(MeCN)_4]$-ClO_4, Cu^I, even if facing a large excess of L∩L, does not form the $[Cu^I(L∩L)_2]^+$ complex, in which the metal should be coordinated to one bidentate imine-pyridine subunit of each molecule of L∩L, but prefers to give immediately the 2:2 helicate complex. Figure 3b reports as an example absorbance values at 600 nm, pertaining to the higher energy MLCT band, which fit well the concentration profile of the $[Cu^I_2(L∩L)_2]^{2+}$ complex.

In an opposite experiment, an MeCN solution of $Cu^I(MeCN)_4ClO_4$ was titrated with a standard solution of L∩L. The family of spectra taken in the titration are shown in Figure 4a.

Addition of L∩L induces the development of the already observed spectrum of the $[Cu^I_2(L∩L)_2]^{2+}$ helicate complexes, whose MLCT bands reach a limiting absorbance for an L/Cu^I molar ratio of 1. Figure 4b shows the calculated concentration profiles of the species at equilibrium over the course of the titration: Cu^I, $[Cu^I_2(L∩L)_2]^{2+}$, and L∩L. Also in the present case, absorbance values in the MLCT spectral region fit well the concentration of the concentration profiles of the $[Cu^I_2(L∩L)_2]^{2+}$ complex. Excess addition of L∩L does not induce any significant spectral modification, which suggests integrity of the dimetallic complex, with respect to the formation of the $[Cu^IL_2]^+$ complex.

It has to be noted that analogous titration experiments with helicands ^{RR}2 and ^{RR}3 indicated the occurrence of both equilibria 1 and 2 and pertinent log *K* values are reported in Table 2. The stability of the helicate complexes (expressed by log K_{22}) varies according to the sequence ^{RR}2 > ^{RR}3 ≈ ^{RR}4, which may reflect the interstrand steric repulsions exerted by the −OR substituents at the quinoline ring. These unfavorable effects probably cancel the exergonic contributions deriving from interstrand π−π interactions present in the $[Cu^I_2(^{RR}3)_2]^{2+}$ complex (2 interactions) and in the $[Cu^I_2(^{RR}4)_2]^{2+}$ complex (4 interactions). In this connection, it should mentioned that the π−π interactions observed in the solid state may not necessarily be maintained in solution because of the free rotation of the naphthyl groups, with the consequence that the strength of the π−π contacts between the phenyl groups and napthyl groups might be similar.

We now have to explain why, in excess of L∩L, the mononuclear complex $[Cu^I(L∩L)_2]^+$ forms with ^{RR}2 and ^{RR}3, whereas in the case of ^{RR}4 such a complex does not form and the dinuclear helicate complex is immediately obtained when adding Cu^I to an excess of L∩L and does not decompose on addition of excess addition of L∩L to Cu^I. A possible explanation could refer to the significant repulsive effects exerted by the naphthylmethoxy substituent present in the ^{RR}4 ligand compared to ^{RR}2 and ^{RR}3. To evaluate the extent of such repulsions, we considered the interaction equilibria of Cu^I with two related bidentate ligands: **6**, which can be considered as a half of the helicand ^{RR}4, bearing the naphthylmethoxy substituent, and **5**, which does not contain any substituent at the quinoline subunit and should therefore exert minimum repulsive interactions.

Figure 5a shows the family of spectra recorded over the course of the titration in MeCN of a solution 1.006×10^{-4} M in $[Cu^I(MeCN)_4]ClO_4$ with a solution 1.014×10^{-2} M in **6**.

dx.doi.org/10.1021/ic401684u | *Inorg. Chem.* 2013, 52, 10643−10652

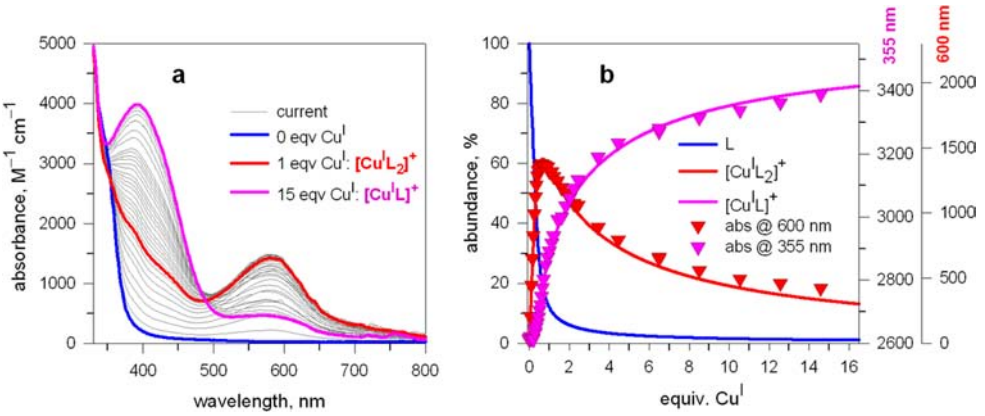

Figure 6. (a) Absorption spectra taken over the course of the titration of an MeCN solution 1.014×10^{-2} M of **6** with a standard solution of $[Cu^I(MeCN)_4]ClO_4$ 1.006×10^{-4}; (b) lines: concentration profiles (% with respect to Cu^I) of the species at the equilibrium; symbols: molar absorbances at 600 nm (red) and at 355 nm (pink).

On addition of **6**, an intense band centered at 580 nm develops, of MLCT nature, reflecting the interaction of Cu^I with the imine-pyridine ligand. Best fitting of titration data, over the 400−750 nm interval was obtained by assuming the occurrence of the stepwise equilibria 3 and 4, to which the following log K values, log K'_{11} = 4.83 ± 0.01 and log K'_{21} = 4.62 ± 0.01, correspond,

$$Cu^+ + \mathbf{6} \leftrightarrows [Cu^I\mathbf{6}]^+ \quad \log K'_{11} \tag{3}$$

$$[Cu^I\mathbf{6}]^+ + \mathbf{6} \leftrightarrows [Cu^I(\mathbf{6})_2]^+ \quad \log K'_{21} \tag{4}$$

Concentration profiles shown in Figure 5b indicate that the 1:1 complex $[Cu^I(\mathbf{6})]^+$ forms on first addition of **6**, to reach its maximum concentration (∼ 30%) on addition of 1 equiv of ligand (it is hypothesized that the other two coordination sites of the tetrahedron are occupied by MeCN molecules). On further addition of **6**, the 2:1 complex is obtained. To obtain a more significant concentration of the 1:1 complex, the reverse titration experiment was carried out. In particular, a solution 1.006×10^{-4} M of **6** was titrated with a standard solution of $[Cu^I(MeCN)_4]ClO_4$ 1.014×10^{-2} M.

Figure 6a shows the family of spectra obtained over the course of the titration. On the very first addition of Cu^I, the band at 580 nm forms, pertinent to the $[Cu^I(\mathbf{6})_2]^{2+}$ complex, which reaches its highest intensity at 1 equiv of the metal salt. On further addition of Cu^I, the band at 580 nm smoothly decreases, while a new band develops centered at 390 nm. The latter absorption must be ascribed to the $[Cu^I(\mathbf{6})]^{2+}$ complex, in which tetrahedral coordination is completed by two MeCN molecules. A best fit of the titration data over the 350−800 nm interval through a nonlinear least-squares procedure was obtained by assuming the occurrence of equilibria 3 and 4, to which the following constants correspond log K'_{11} = 4.78 ± 0.01, log K'_{21} = 4.92 ± 0.01. These values are in satisfactory agreement with those obtained from the reverse titration illustated in Figure 5a, which validates the reliability of the model. Table 2 displays the average values of log K' values from the two experiments. It is observed that log K'_{11} (eq 3) and log K'_{21} (eq 4) are coincident within the experimental uncertainty, which suggests that the two bulky substituents, in a tetrahedral geometrical arrangement, do not exert any particular repulsive effect. This suggests also that interstrand steric repulsions should be minimally significant also in the Cu^I/**4** system and that, therefore, failure in the formation of the $[Cu^I(\mathbf{4})_2]^{2+}$ complex has to be solely attributed to the extra stability of the helicate arrangement associated to the presence of 4 well-defined interstrand $\pi-\pi$ interactions.

For comparative purposes, similar spectrophotometric titration experiments have been carried out also on the Cu^I/**5** system, in which no substituents are present in the 8 position of the quinoline moiety (see Supporting Information, Figures S2 and S3). On titration of a 1.023×10^{-4} M solution of $[Cu^I(MeCN)_4]ClO_4$ with a standard solution of **5**, the following equilibrium constant were obtained: log K'_{11} = 5.07(4) and log K'_{21} = 5.07(8). On the other hand, in the reverse titration (a 1.005×10^{-4} M solution in **5** titrated with a solution of of $[Cu^I(MeCN)_4]ClO_4$) the same log K values were obtained: log K'_{11} = 5.11(2) and log K'_{21} = 5.07(5). Pertinent spectra and concentration profiles of the species at the equilibrium are show in Supporting Information, Figures S2 and S3. The coincidence of the log K_{11} and log K_{22} values reinforces the observation that repulsive effects do not operate in the formation of the $[Cu^IL_2]^+$ complex, with L obtained through Schiff base condensation of unsubstituted quinoline carbaldehyde and cyclohexylamine.

At this stage, to elucidate the factors governing the stability of the helicate complex, it can be useful to compare the two reactions:

$$2Cu^I + 2\,\mathbf{4} \leftrightarrows [Cu^I{}_2(\mathbf{4})_2]^{2+} \quad \log K = \log K_{22} = 16.1 \tag{5}$$

$$2Cu^I + 4\,\mathbf{6} \leftrightarrows 2[Cu^I(\mathbf{6})_2]^+ \quad \log K = 2 \times (\log K'_{11} + \log K'_{21}) = 19.2 \tag{6}$$

The comparison is homogeneous because both equilibria lead to the establishing of four Cu^I−N bonds. However, it is observed that the formation of two mononuclear complexes $[Cu^I(\mathbf{6})_2]^+$ is favored by 3 orders of magnitude with respect to that involving the helicate $[Cu^I{}_2(\mathbf{4})_2]^{2+}$. We were not able to grow crystals of the $[Cu^I(\mathbf{6})_2]ClO_4$ complex suitable for X-ray diffraction studies. However, we can assume that the structural features of the $[Cu^I(\mathbf{6})_2]^+$ complex are not too different from those of the analogous, crystallographically analyzed $[Cu^I(\mathbf{7})_2]^+$ complex, in which pyridine, rather than quinoline rings are present.[15]

The complex shows a slightly distorted tetrahedral coordination geometry. In particular, the planes containing the penta-atomic chelate rings forms an angle θ = 82.5° (regular

dx.doi.org/10.1021/ic401684u | Inorg. Chem. 2013, 52, 10643−10652

tetrahedral geometry: θ = 90°). On the other hand, in the helicate complex $[Cu^{I}_2(\mathbf{4})_2]^{2+}$, θ angles are 72.6° and 70.8°, indicating a substantial deviation from the tetrahedral geometry and suggesting the presence of significant steric constraints within the ligating framework. Thus, it can be hypothesized that the higher value of log K for eq6 with respect to eq5, which corresponds to 4.2 kcal mol^{-1}, mostly reflects the higher strength of the Cu^{I}–N bond interactions in the less strained mononuclear complexes (enthalpy contribution). Thus, the stability of the $[Cu^{I}_2(\mathbf{4})_2]^{2+}$ helicate complex, which resists the addition of a large excess both of bis-bidentate ligand and of Cu^{I}, should result from an especially favorable entropy effect. Such an effect should originate from the statistically favored uptake of the second Cu^{I} ion by the second bidentate subunits of **4** with respect to the complexation by two different molecules of helicand coming from the solution. On this basis, the helicate effect should increase with the dilution. In this sense, the helicate effect shows a significant analogy with the chelate effect.

3. Interaction of Cu^{II} with ^{RR}4 and the Cu^{II}/Cu^{I} Redox Change. The related helicand **1** forms a mononuclear complex of stoichiometry 1:1 with Cu^{II}, with a slightly distorted square geometry as ascertained by X-ray studies. This depends mainly by the Ligand Field Energy advantage experienced by a d^9 metal center in a tetragonal coordination geometry. On the other hand a square polygon does not exhibit any helical twist, as the tetrahedron and the octahedron solids do. On the other side, Cu^{II} forms with **3** a crystalline 2:2 complex, $[Cu^{II}_2(\mathbf{3})_2]^{4+}$, with a double strand helical structure, in which each Cu^{II} metal center is six-coordinated according to a cis-octahedral geometry and interacts with a NNO donor subunit of each strand, the oxygen atom being that of the benzyloxy substituent. However, such a helicate complex is not stable in an MeCN solution, where it completely disassembles to give two mononuclear complexes, as clearly shown by ESI mass studies.

We were unfortunately not able to obtain crystal suitable for X-ray diffraction studies from solutions containing equimolar amounts of ^{RR}**4** and of a Cu^{II} salt (triflate, perchlorate). Thus, we investigated the formation of the Cu^{II}/^{RR}**4** complex in solution by titrating a solution 1.02×10^{-4} M in ^{RR}**4** with a standard solution of Cu$^{II}(CF_3SO_3)_2$ (1.00×10^{-2} M). Figure 7a shows the family of spectra obtained over the course of the titration.

The uncomplexed ligand ^{RR}**4** shows an intense absorption band at 310 nm, with a shoulder at 350 nm, assigned to transitions within the imine-pyridine system (red line). On Cu^{II} addition, the two bands are significantly red-shifted, as a consequence of the interaction of the metal ion with imine and pyridine nitrogen atoms, while the solution takes on a bright yellow color. The titration profile based on the absorbance at 345 nm, shown in Figure 8b, clearly indicates the formation of a complex species with 1:1 metal/ligand ratio. Such a value is consistent with the formation of both the mononuclear $[Cu^{II}(\mathbf{5})]^{2+}$ and the dinuclear $[Cu^{II}_2(\mathbf{5})_2]^{4+}$ complex. The absence of curvature in the profile indicates the formation of an especially stable complex ($K \geq 10^6$ for the mononuclear species) and in any case ensures that, in a solution containing equimolar amounts of metal and ligand, in the investigated range of concentration the complex is present at 100%.

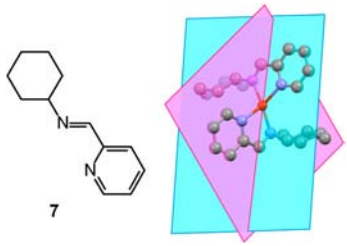

Figure 7. Crystal structure of the model complex $[Cu^{I}(\mathbf{7})_2]^{+}$,[15] showing the planes containing the five-membered chelate rings Cu–N–C–C-N. The two planes form an angle θ = 82.5°, thus indicating a moderate distortion from the tetrahedral coordination geometry (for a regular tetrahedron θ = 90°).

The ESI mass spectrum of an MeCN solution containing equimolar amounts of ^{RR}**4** and $Cu(CF_3SO_3)_2$ showed a peak at 768.7 m/z, corresponding to the species $[Cu^{I}_2(^{RR}\mathbf{4})2]^{2+}$. In particular, the isotope pattern showed a peak-to-peak separation of 0.5 m/z and the presence of two copper ions. No doubt that under the drastic conditions of the experiment Cu^{II}-to-Cu^{I} reduction takes place. However, at this stage, we cannot assess whether the reduction involves a dicopper(II) complex or a mononuclear Cu^{II} species, which, after reduction, assemble to give the helicate complex. More direct pieces of information on the nature of the Cu^{II}/^{RR}**4** system in solution came from voltammetric studies (vide infra).

We first investigated the oxidation behavior of the $[Cu^{I}_2(\mathbf{4})_2]^{2+}$ complex in an MeCN solution through cyclic voltammetry (CV) studies at a platinum working electrode. Figure 9a (red solid line) shows the CV profile obtained over the range of potential −200 mV/800 mV (vs Fc^{+}/Fc), taken at a potential scan rate of 100 mV s^{-1}.

The voltammogram shows on the oxidation scan two well-defined waves, fully reversible in the reverse scan, with a peak separation of 58 mV for each wave. The following half-wave potentials were calculated $E_{1/2}(1)$ = 180 mV and $E_{1/2}(2)$ = 442 mV, with a ΔE_{CV} = 262 mV. The CV response results from the two following half-reactions:

$$[Cu^{I}_2(\mathbf{4})_2]^{2+} \leftrightarrows [Cu^{I}Cu^{II}(\mathbf{4})_2]^{3+} + e^{-} \quad (7)$$

$$[Cu^{I}Cu^{II}(\mathbf{4})_2]^{3+} \leftrightarrows [Cu^{II}Cu^{II}(\mathbf{4})_2]^{4+} + e^{-} \quad (8)$$

Full reversibility of the CV profile indicates that the mixed valence $[Cu^{I}Cu^{II}(\mathbf{4})_2]^{3+}$ and the fully oxidized $[Cu^{II}Cu^{II}(\mathbf{4})_2]^{4+}$ complex maintain their integrity and the double strand helicate arrangement in the time scale of the CV experiment. This is confirmed by Differential Pulse Voltammetry studies on the same solution (Figure 9b). Two symmetric peaks are observed, with a peak-to-peak separation ΔE_{DPV} = 260 mV. Peak width at half heigth is 105 mV for each peak.

The ΔE value is associated to the comproportionation process

$$[Cu^{I}_2(\mathbf{4})_2]^{2+} + [Cu^{II}Cu^{II}(\mathbf{4})_2]^{4+} \leftrightarrows 2[Cu^{I}Cu^{II}(\mathbf{4})_2]^{3+} \quad (9)$$

The higher ΔE, the more favored the comproportionation process. In particular,

$$K_C = \exp\left(\frac{\Delta E \times F}{R \times T}\right) \quad (10)$$

[at 298K, $K_C = \exp(\Delta E/25.69)$ when ΔE is expressed in mV].[16]

Three main terms may contribute to ΔE, thus to the magnitude of the comproportionation constant K_C, as ex-

dx.doi.org/10.1021/ic401684u | Inorg. Chem. 2013, 52, 10643−10652

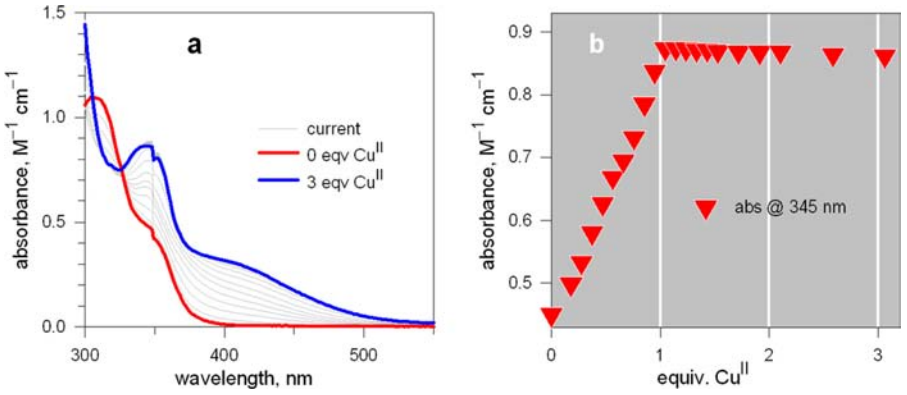

Figure 8. (a) Family of spectra recorded over the course of the titration of a 1.00×10^{-4} solution of *rac*-**5** with a 1.0×10^{-2} MeCN solution of $Cu^{II}(CF_3SO_3)_2$. Red line, spectrum of ^{RR}**4** prior to the titration; gray lines, current spectra; blue line, spectrum after the addition of 3 equiv of Cu^{II}; (b) titration profile based on the absorbance at 345 nm.

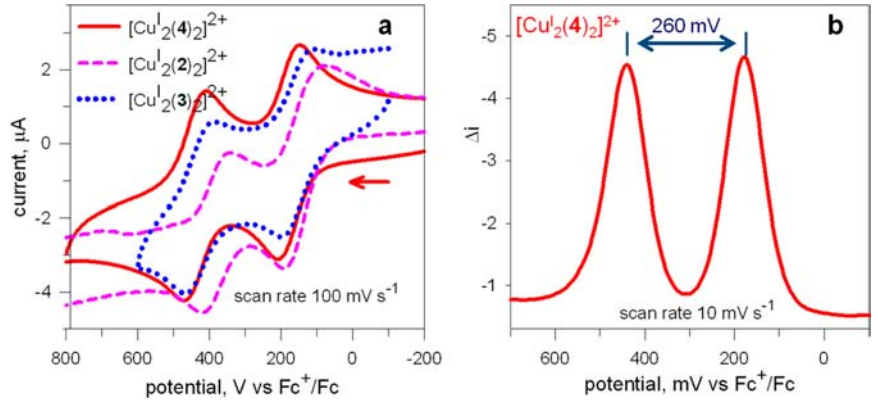

Figure 9. (a) CV profile taken at a platinum working electrode at a potential scan rate of 100 mV s^{-1} on a MeCN solution of $[Cu^I_2(4)_2](ClO_4)_2$, made 0.1 M in $[Bu_4N]PF_6$ (solid red line); dashed lines refer to $[Cu^I_2(2)_2]^{2+}$ (pink) and $[Cu^I_2(3)_2]^{2+}$(blue) complexes, investigated under the same conditions; (b) Differential Pulse Voltammetry profile taken on the same solution of $[Cu^I_2(4)_2](ClO_4)_2$ (potential scan rate 10 mV s^{-1}).

pressed by eq 10: (i) the statistical factor with 35.61 mV; (ii) an electrostatic term, which takes into account the Coulombic repulsions between metal ions in the two sides of the comproportionation equilibrium 9. In particular, in the left side the following repulsions operate $(1 \times 1) + (2 \times 2) = 5$ positive charges, whereas in the right side the number positive charges amounts to $4 = 2 \times (1 \times 2)$, a circumstance which favors the displacement of eq 9 to the right; (iii) a magnetic interaction between two metal centers in a given oxidation state: this could be the case of Cu^{II} (d^9) ions, which possess one unpaired electron and are therefore prone to spin pairing, but the large distance between metal centers and the absence of any bridging ligand preclude magnetic interaction. Thus, the magnitude of ΔE should be essentially controlled by the repulsive electrostatic term.

In Figure 10, ΔE values for $[Cu^I_2(2)_2]^{2+}$, $[Cu^I_2(3)_2]^{2+}$, and $[Cu^I_2(4)_2]^{2+}$ complexes are plotted vs the Cu^I–Cu^I distance, showing a roughly linear increase. Such a relationship is counterintuitive. In fact, one would expect that the electrostatic repulsion between cations, thus the favorable Coulombic contribution to ΔE, decreases with the increasing intermetallic distance, whereas the opposite behavior is observed. However, it should be considered that the Cu^I–Cu^I repulsion is a minor term with respect to Cu^{II}–Cu^{II} repulsion. Thus, a ΔE vs Cu^{II}–Cu^{II} distance could be probably more significant. Moreover, the reversibility of the CV profiles indicates that the Cu^I,Cu^{II} and Cu^{II},Cu^{II} complexes maintain a double strand helicate structure,

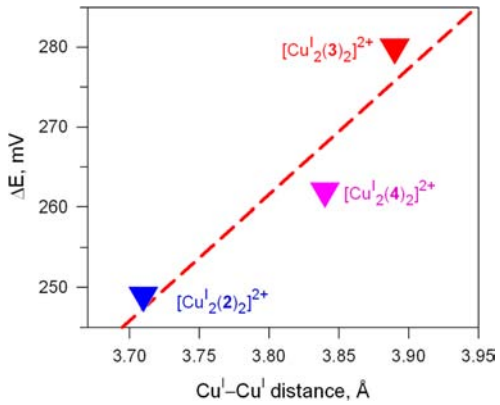

Figure 10. Plot of ΔE ($= E_{1/2}(2) - E_{1/2}(1)$ in Figure 9a) vs the crystallographically determined Cu^I–Cu^I distance in $[Cu^I_2(L\cap L)_2](ClO_4)_2$ complex salt (L∩L = **2**,[7f] **3**,[8] **4**).

but a fine geometrical rearrangement of the donor set around the Cu^{II} center cannot be excluded, which can modify to a different extent both the intermetallic distance and the effective electrical charge of each dication.

Figure 11 shows the CV profile obtained for an MeCN solution equimolar in **4** and in $Cu^{II}(CF_3SO_3)_2$, and made 0.1 M in $[Bu_4N]PF_6$, at a potential scan rate of 100 mV s^{-1} (solid red line). For comparative purposes, CV profiles obtained under

dx.doi.org/10.1021/ic401684u | *Inorg. Chem.* 2013, 52, 10643−10652

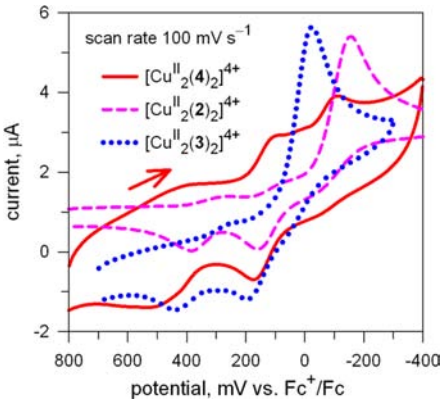

Figure 11. CV profile taken at a platinum working electrode at a potential scan rate of 100 mV s^{-1} on a MeCN solution equimolar in $Cu^{II}(CF_3SO_3)_2$ and ^{RR}**4**, made 0.1 M in $[Bu_4N]PF_6$ (solid red line); dashed lines refer to Cu^{II}/**2** (pink dashed line) and Cu^{II}/**3** (blue dashed line) systems, investigated under the same conditions.

the same conditions for **2** (pink dashed line) and **3** (blue dashed line) are reported.

It is convenient to discuss first the CV profiles obtained for solutions containing systems Cu^{II}/**2** and Cu^{II}/**3** (in which both metal and ligand are present in equimolar amounts). For these systems, ESI mass studies had assessed that Cu^{II} was solely present as a mononuclear complex of 1:1 stoichiometry: $[Cu^{II}(\mathbf{2})]^{2+}$ and $[Cu^{II}(\mathbf{3})]^{2+}$. On the reduction scan, a single peak is observed for both complexes, which is assigned to the one electron reduction half-reaction 11:

$$[Cu^{II}(L \cap L)]^{2+} + e^- \leftrightarrows [Cu^{I}(L \cap L)]^{+} \quad (11)$$

On the reverse oxidation scan, two well-defined peaks develop separated by about 250 mV. This suggest that two $[Cu^{I}(L\cap L)]^{+}$ complexes, prior to the oxidation scan, assemble to give the double strand helicate complex, which undergoes two stepwise oxidation processes.

The Cu^{II}/**4** system displays a different behavior. Also in the reduction scan, two waves are observed, which are maintained also in the reverse oxidation scan. This suggests that in the solution equimolar in Cu^{II} and **4**, metals and ligands assemble to give a dimeric species, probably arranged in a double helical structure. A double strand helicate arrangement had been observed in the crystalline $[Cu^{II}_2(\mathbf{3})_2](CF_3SO_3)_4$,[8] in which each metal center experienced six-coordination by a 2 × N_2O donor set. In that case, the helicoidal arrangement was reinforced by $\pi-\pi$ interactions between the benzyloxy substituent of one strand with the quinoline subunit of the other strand. It has been already mentioned that these interactions were not strong enough to prevent disassembling in solution. It is possible that more intense $\pi-\pi$ interstrand interactions are established between each quinoline subunit and each naphthylmethoxy moiety, which impart a higher stability to the helicate arrangement and guarantees integrity in solution of the $[Cu^{II}_2(\mathbf{4})_2]^{4+}$ complex. This may also explain the detection of the dimetallic species $[Cu^{I}_2(\mathbf{4})_2]^{2+}$ in the ESI mass experiment, which is probably obtained by reduction of the dicopper(II) complex present in solution. On the other hand, reduction of the mononuclear $[Cu^{II}(\mathbf{4})]^{2+}$ species to $[Cu^{I}(\mathbf{4})]^{+}$ and the consecutive assembly to give the dimetallic $[Cu^{I}_2(\mathbf{4})_2]^{2+}$ complex seems a more complicated and less probable event.

CONCLUSION

The bis-bidentate ligand ^{RR}**4** forms with Cu^{I} an especially stable helicate complex, $[Cu^{I}_2(\mathbf{4})_2]^{2+}$, whose strands are held together by 8 Cu^{I}–N coordinative bonds and by 4 additional $\pi-\pi$ intracomplex interactions, involving a quinoline subunit of one strand and a naphthylmethoxy substituent of the other strand. This imparts an especially high stability to the helicate complex, which does not decomposes on addition of an excess either of the helicand ^{RR}**4** or of the Cu^{I} ion. Comparison of log *K* values of formation equilibria of the helicate complex $[Cu^{I}_2(^{RR}\mathbf{4})_2]^{2+}$ and of the complex with the half-helicand **6** illuminates the nature of the helicate effect, which is solely entropic.

CV studies on an MeCN solution of $[Cu^{I}_2(^{RR}\mathbf{4})_2]^{2+}$ showed the occurrence of two reversible consecutive one-electron oxidation processes separated by a ΔE = 260 mV, which emphasizes the stability of the mixed valence complex $[Cu^{I}Cu^{II}(^{RR}\mathbf{4})_2]^{3+}$. The stability of the mixed valence species with respect to the disproportionation to $[Cu^{I}_2(^{RR}\mathbf{4})_2]^{2+}$ and $[Cu^{II}_2(^{RR}\mathbf{4})_2]^{4+}$ complexes seems to be solely ascribed to an electrostatic effect.

Titration of an MeCN solution of ^{RR}**4** with a solution of $Cu^{II}(CF_3SO_3)_2$ showed a sharp equivalent point at a 1:1 stoichiometric ratio, corresponding to the formation both of a mononuclear and of a dinuclear complex. However, CV profiles for a solution containing equimolar amounts of **4** and Cu^{II} showed two definite waves in the reduction scan, separated by about 250 mV, and two definite waves in the reverse scan, still separate by about 250 mV. This suggests the presence in solution of a dinuclear complex of copper(II), $[Cu^{II}_2(^{RR}\mathbf{4})_2]^{4+}$, whose unusual stability, never observed with bis-bidentate ligands obtained by Schiff base condensation of 1,2-diaminecyclohexane, should be ascribed to existence of interstrand $\pi-\pi$ interactions.

This work has demonstrated that the formation of double-strand helicate complexes can be favored by taking advantage of $\pi-\pi$ interactions involving chosen subunits of each strand. In particular, subunits of definite π-donor and π-acceptor tendencies can be chosen to design especially stable and robust helicates of both Cu^{I} (usual) and Cu^{II} (less usual) cations, displaying a multielectron redox behavior.

ASSOCIATED CONTENT

Supporting Information

X-ray crystallographic files in CIF format for the $[Cu_2^{I}(^{RR}\mathbf{4})_2](ClO_4)_2\cdot 4CH_3CN\cdot 2H_2O$ complex salt. Details on the spectrophotometric titrations in MeCN for the interaction of Cu^{I} with **5**. This material is available free of charge via the Internet at http://pubs.acs.org.

AUTHOR INFORMATION

Corresponding Author

*E-mail: luigi.fabbrizzi@unipv.it.

Notes

The authors declare no competing financial interest.

ACKNOWLEDGMENTS

The financial support of the Italian Ministry of University and Research (PRIN–InfoChem) is gratefully acknowledged.

REFERENCES

(1) Watson, J. D.; Crick, F. H. C. *Nature* **1953**, *171*, 737–738.

(2) Lehn, J.-M.; Rigault, A.; Siegel, J.; Harrowfield, J.; Chevrier, B.; Moras, D. *Proc. Natl. Acad. Sci. U.S.A.* **1987**, *84*, 2565−2569.
(3) Albrecht, M. *Chem. Rev.* **2001**, *101*, 3457−3497.
(4) (a) Garrett, T. M.; Koert, U.; Lehn, J.-M.; Rigault, A.; Meyer, D.; Fischer, J. *Chem.Commun.* **1990**, 557−558. (b) Barley, M.; Constable, E. C.; Corr, S. A.; McQueen, R. C. S.; Nutkins, J. C.; Ward, M. D.; Drew, M. G. B. *J. Chem. Soc., Dalton Trans.* **1988**, 2655−2662. (c) Piguet, C.; Bernardinelli, G.; Williams, A. F. *Inorg. Chem.* **1989**, *28*, 2920−2925.
(5) Van Stein, G. C.; Van der Poel, H.; Van Koten, G.; Spek, A. L.; Duisenberg, A. J. M.; Pregosin, P. S. *J. Chem. Soc., Chem. Commun.* **1980**, 1016−1018.
(6) Amendola, V.; Fabbrizzi, L.; Linati, L.; Mangano, C.; Pallavicini, P.; Pedrazzini, V.; Zema, M. *Chem.−Eur. J.* **1999**, *5*, 3679−3688.
(7) (a) Amendola, V.; Fabbrizzi, L.; Mangano, C.; Pallavicini, P.; Roboli, E.; Zema, M. *Inorg. Chem.* **2000**, *39*, 5803−5806. (b) Amendola, V.; Fabbrizzi, L.; Pallavicini, P. *Coord. Chem. Rev.* **2001**, *216−217*, 435−448. (c) Amendola, V.; Fabbrizzi, L.; Gianelli, L.; Maggi, C.; Mangano, C.; Pallavicini, P.; Zema, M. *Inorg. Chem.* **2001**, *40*, 3579−3587. (d) Amendola, V.; Fabbrizzi, L.; Pallavicini, P.; Sartirana, E.; Taglietti, A. *Inorg. Chem.* **2003**, *42*, 1632−1636. (e) Amendola, V.; Fabbrizzi, L.; Mundum, E.; Pallavicini, P. *Dalton Trans.* **2003**, 773−774. (f) Pallavicini, P.; Boiocchi, M.; Dacarro, G.; Mangano, C. *New J. Chem.* **2007**, *31*, 927−935.
(8) Amendola, V.; Boiocchi, M.; Brega, V.; Fabbrizzi, L.; Mosca, L. *Inorg. Chem.* **2010**, *49*, 997−1007.
(9) Hathaway, J.; Holah, D. G.; Postlethwaite, J. D. *J. Chem. Soc.* **1961**, 3215−3218.
(10) *SAINT Software Reference Manual*, Version 6; Bruker AXS Inc.: Madison, WI, 2003.
(11) Sheldrick, G. M. *SADABS Siemens Area Detector Absorption Correction Program*; University of Göttingen: Göttingen, Germany, 1996.
(12) Altomare, A.; Burla, M. C.; Camalli, M.; Cascarano, G. L.; Giacovazzo, C.; Guagliardi, A.; Moliterni, A. G. G.; Polidori, G.; Spagna, R. *J. Appl. Crystallogr.* **1999**, *32*, 115−119.
(13) Sheldrick, G. M. *Acta Crystallogr.* **2008**, *A64*, 112−122.
(14) Hyperquad package; Gans, P.; Sabatini, A.; Vacca, A. *Talanta* **1996**, *43*, 1739−1753. http://www.hyperquad.co.uk/index.htm; accessed 28 June, 2013.
(15) Massa, W.; Dehghanpour, S.; Jahani, K. *Inorg. Chim. Acta* **2009**, *362*, 2872−2878.
(16) Richardson, D. E.; Taube, H. *Inorg. Chem.* **1981**, *20*, 1278−1285.